RSC Advances

ROYAL SOCIETY OF CHEMISTRY

www.rsc.org/advances

Polydopamine and graphene oxide synergistically modified prussian blue electrochemical immunosensor for the detection of alpha-fetoprotein with enhanced stability and sensibility

Ren-zhong Zhang, Bo-guang Pan, Hai-ning Wang, Jian-ming Dan, Cheng-lin Hong, Hong-ling Li*

College of Chemistry and Chemical Engineering, Shihezi University

Key Laboratory for Green Processing of Chemical Engineering of Xinjiang Bingtuan, Shihezi 832000, China

Corresponding author: Professor, Hongling Li; lhl_tea@shzu.edu.cn (China); North Quad 221, Shihezi City, Xinjiang Uygur Autonomous Region

Abstract

In this paper, a simple and highly sensitive amperometric immunosensor for the determination of alpha-fetoprotein (AFP) based on multi-functional gold nanoparticles-polydopamine-Prussian Blue-graphene oxide nanocomposites (Au-PDA-PB-GO) was fabricated. GO as a template was employed to situ synthesized PB nanoparticle, then PB-GO surface was functionalized by one-step oxidative polymerization of dopamine in basic solution at environment friendly condition to obtain the polydopamine (PDA) modified reduced PB-GO nanoparticles. Via in situ deposition, the Au NPs deposited on the polydopamine functionalized PB-GO nanocomposites. The Au-PDA-PB-GO nanocomposites not only enhance the stability of prussian blue and provided a favorable microenvironment to maintain the activity of the immobilized biomolecules due to the excellent biocompatibility of PDA, but also increased the loading capacity of the biomolecules due to the large surface area of nanocomposites, and the present of gold nanoparticles enhanced the conductivity and charge-transport properties of the composites. The dynamic range of the resulted immunosensor for the detection of AFP is from 0.01 ng/ml to 80.0 ng/ml with a detection limit of 0.007 ng/ml (S/N=3). Moreover, this biosensor displays good selectivity, stability and reproducibility.

Keywords: polydopamine, prussian blue, graphene oxide, gold nanoparticles, immunosensor

1. Introduction

Hepatocellular Carcinoma (HCC) is one of the world's most common cancers.[1] Early liver cancer is closely associated with some specific proteins called tumor markers. Alpha-fetoprotein (AFP) is one of the specific tumor markers of HCC.[2, 3] Therefore, simply and rapidly detect the concentration of AFP has vital significance for the early diagnosis of liver cancer. Electrochemical immunosensors are widely noticed since they are simple, sensitive and specific.[4] Nanocomposites have stimulated intense research over past decades due to their high biocompatibility and large surface area.[5] Various nanocomposites with different structures and constitutions have been synthesized and applied to tumor markers detection in recent years, such as gold nanoparticles (Au NPs),[5-7] carbon nanotubes (CNTs) [6,8], ordered mesoporous carbons (OMCs),[9] polydopamine (PDA),[10-12] Graphene Oxide (GO),[13-15] CuO nanoparticles,[16] Cu_2O nanoparticles,[17] prussian blue (PB) [18] etc. With the nanostructured materials, enhanced electrochemical activity and increased surface area have been proved practicable in the previous studies.

Wherein the maintenance of stability and electrocatalytic activity after electroactive materials are modified on electrode surface has become one of the hottest research point.[19, 20] Take prussian blue nanoparticles (PB NPs), which is a hexacyanoferrate with a face-centered cubic lattice structure, it has been widely used as electronic media content in the electrochemical biosensor because of it's excellent electrocatalytic properties, electrochemical reversibility, easy preparation and high thermal stability.[21-24] However, the PB NPs modified electrochemical biosensor usually show short lifetime and poor stability as the water solubility of PB NPs, and it easy to be destroyed and lost activity in weak alkaline environment, it is limited as the electronic media immunosensor.

Dopamine (DA), a catecholamine neurotransmitter, has excellent biocompatibility [25] and self-polymerizing ability.[26, 27] Hong et al. reported that stable polydopamine (PDA) is formed by non-covalent self-assembly and Covalent Polymerization.[28] After the polymerization reaction, the residual catechol groups of the PDA film can produce an extremely versatile platform for the immobilization of biological molecules and the possible in situ deposition of metallic nanoparticles.[29, 30] Recently, due to its prominent advantages, PDA has been regarded as a mild and efficient method for modifying various surfaces through a simple dipping treatment [31] and ameliorating the surface

characteristics such as biocompatibility [25] and wettability.[32]

At present, the graphene materials for electrochemical sensor is mainly prepared by GO solution reduction method.[33] Compared with other methods (micro mechanical stripping method, chemical vapor deposition, epitaxial growth method), GO solution reduction method has the advantages of simple operation, high yield and low cost. After the reaction of GO, which not only has good conductivity and high specific surface area, and contains some structural defects and a small amount of functional groups, and is an ideal electrode material. Currently, the reduction methods of GO include: chemical reduction method (reducing agent comprises two hydrazine, methylhydrazine, sodium borohydride, hydroquinone, sulfur-containing compounds and so on), electrochemical reduction, thermal reduction method and UV assisted reduction method. And the RGO in electrochemical sensor is mainly chemically reduced graphene oxide (CRGO) and electrochemically reduced of graphene oxide (ERGO).

In 2006, Ruoff [34] for the first time by using hydrazine as reducing agent, through GO solution chemical reaction to prepare a single layer graphene, known as Chemically Reduced Graphene Oxide (CRGO).Through the electrochemical reduction of GO to get the ERGO, there are mainly two kinds of methods. One is a two step electrochemical reduction, which first put GO through surface droplets coated or immersion methods to modify the electrode, then the electrochemical reduction reaction.[35-37] Another method is the reduction of GO by one step electrochemical electrode, which is directly inserted into the GO solution, and then use the cyclic voltammetry or constant voltage deposition method to reduce GO and do the surface modification to the electrode.[38,39] In recent years, the detection of electrochemical sensor based on ERGO has been widely applied in small molecule.[40-42] In experimental study, mainly uses the modified Hummers method for the synthesis of water soluble graphene oxide.[43,44]

Graphene oxide, owe to these advantageous physicochemical and structural properties, GO proved to be a hopeful material in designing and preparing electroactive nanocomposites. Han et al. reported a one-step approach to synthesize graphene oxide–thionine–Au (GO–Thi–Au) nanocomposites using the synergistic effect of Thi and GO and the immunosensor showed an ultralow detection limit of 0.05 fg ml^{-1}.[45] Cao et al. used the cube PB NPs to deposit on the surface of graphene oxide, and the

nanocomposite showed better conductivity and resistance to acid and base. [46]

In this work, we report a sensitive AFP immunosensor based on multi-functional gold nanoparticles-polydopamine-Prussian Blue-graphene oxide nanocomposites (Au-PDA-PB-GO). GO as a template was employed to situ synthesized PB nanoparticle, then PB-GO surface was functionalized by one-step oxidative polymerization of dopamine in basic solution at environment friendly condition to obtain the polydopamine (PDA) modified reduced PB-GO nanoparticles. Via in situ deposition, the Au NPs deposited on the polydopamine functionalized PB-GO nanocomposites. The Au-PDA-PB-GO nanocomposites not only enhance the stability of prussian blue and provide a favorable microenvironment to maintain the activity of the immobilized biomolecules due to the excellent biocompatibility of PDA, but also increase the loading capacity of the biomolecules due to the large surface area of nanocomposites, and the present of gold nanoparticles enhance the conductivity and charge-transport properties of the composites. By comparison, other detection methods have problems of low stability and repeatability. The fabricated Au-PDA-PB-GO nanocomposites exhibited excellent performance as immunosensors. In addition, the immunosensor is much simpler and lower cost, compared with the sandwich-type immunosensor, because there is no need of secondary incubation.

2. Experimental

2.1. Chemicals and materials

Anti-AFP and AFP were purchased from Biocell Co. (Zhengzhou, China), while Dopamine hydrochloride was from Alfa Aesar. Bovine serum albumin (BSA), Iron (III) chloride hexahydrate ($FeCl_3 \cdot 6H_2O$), potassium ferricyanide ($K_3Fe(CN)_6$) and hydrogen peroxide (H_2O_2) were bought from Sigma. Chloroauric acid ($HAuCl_4 \cdot 4H_2O$) were purchased from Aladdin Chemistry Co. L td. . All other chemicals were of analytical grade and used as received without further purification. Phosphate buffer solution (PBS) of various pH values were prepared by mixing the 1/15 M stock solutions of KH_2PO_4 and Na_2HPO_4 at specific ratios. All solutions were established with ultrapure water (resistivity > 18MΩ/cm).

2.2. Apparatus

Electrochemical impedance spectroscopy (EIS) and cyclic voltammetry (CV) were performed

using a Potentiostat/Galvanostat Model 283 electrochemical workstation (USA) at room temperature. The three-electrode system consisted of bare or modified glassy carbon electrodes (GCE) which was used as a working electrode, a saturated calomel electrode (SCE) as a reference electrode and a Pt wire counter electrode. X-ray powder diffraction (XRD) measurements were performed on a Bruker D8 advanced X-ray diffractometer with Cu-Kα irradiation (λ = 1.5406 Å) at 40 kV and 40 mA in the 2θ scanning range of 10° and 90°. Fourier-transform infrared (FT-IR) spectroscopic were determined using a Nicolet Avatar 360 FT-IR spectrometer. The transmission electron microscope (TEM) images were obtained with a H600 transmission electron microscope (Hitachi Instruments, Japan).

2.3. Synthesis of GO

The GO was synthesized from natural graphite powder based on a modified Hummers method.[47] In brief, 40 mg of graphite powder and 20 mg $NaNO_3$ were added into 1 ml of concentrated H_2SO_4. The mixture was chilled to 0 °C using an ice bath and stirred for 15 min. Then, 0.12 g of $KMnO_4$ was added slowly with temperature controlled below 20 °C. This mixture was allowed to react at 35 °C for 30 min, after which temperature was raised slowly. Subsequently, the mixture was stirred at 98 °C for 15 min. Then, 56 ml ultrapure water and 4 ml of 3% H_2O_2 were added to remove remaining $KMnO_4$. The mixture was allowed to settle before the supernatant was decanted. The remaining mixture was then centrifuged and washed several times alternate with 10% HCl solution and ultrapure water. After vacuum drying at 60 °C, GO sheets was obtained.

2.4. Synthesis of Au-PDA-PB-GO NPs

Take the prepared GO sheets 3mg into 10ml ultrapure water. The mixture was first ultrasonically treated for 10 min to ensure that GO was uniformly dispersed in water. Next, 1 ml of 0.02 M $FeCl_3$ and 0.02 M $K_3Fe(CN)_6$ pH 1.6 bicomponent solution was added slowly, then addition of excess hydrogen peroxide in the reaction. After stirred react at 60 °C for 3 h, PB-GO was obtained. Then take the PB-GO solution into 10 ml pH 6.5 PBS and ultrasonically treated for 10 min. Subsequently, 20 ml pH 6.5 PBS dissolved 30 mg dopamine was added, and the solution was vigorous stirred in ice-water bath for 5 h. After centrifugation and washing with deionized water several times, polydopamine-coated prussian blue-graphene oxide (PDA-PB-GO) nanocomposites were obtained. Next, the Au NPs functionalized PDA-PB-GO nanocomposite was prepared by in situ deposition of Au NPs on the

surface of PDA-PB-GO. In a typical procedure, the obtained PDA-PB-GO solution was dispersed in 1.0 ml 0.1% (w/v) $HAuCl_4$ by ultrasonic. Then 3.0 ml of 1% (w/v) sodium citrate solution was slowly added and stirred for 2 h reaction at room temperature. After another centrifugation and washing thrice with ultrapure water, Au-PDA-PB-GO NPs was prepared and dispersed in 1.0 ml ultrapure water for use. The preparation process is illustrated in Scheme 1(A).

Scheme 1. Procedures for the fabrication of Au-PDA-PB-GO NPs composites(A), and the AFP immunosensor (B)

2.5. Fabrication of the immunosensor

A bare GCE (Φ=4 mm) was first polished to mirror-like smoothness, followed by successive sonicated in ultrapure water, ethanol and ultrapure water for 3 min. After drying the GCE with N_2, 10μL of the Au-PDA-PB-GO solution was carefully dipped onto the pretreated bare GCE surface. After the Au-PDA-PB-GO NPs coated electrode was dried and washed with buffer, thus the Au-PDA-PB-GO NPs modified electrode was obtained. Then, the electrode was incubated in anti-AFP solution at 4°C for 12 h. Then, the electrode was rinsed with ultrapure water to remove the physically absorbed antibodies. Next, the electrode was incubated in 1% BSA solution at 4°C for 2h to block the remaining nonspecific sites on the Au NPs of the functionalized electrode. After the modified electrode was washed carefully with ultrapure water, an immunosensor was fabricated and stored at 4°C when it is not used. The schematic illustration of the stepwise preparation of the immunosensor is shown in Scheme 1(B).

3. Results and discussion

3.1. Characterization of Au-PDA-PB-GO NPs

In this work, dopamine self-polymerization played as a powerful role in applying a layer of multifunctional dopamine film coating on the surface of PB-GO nanocomposite and the subsequent in situ deposition of Au NPs. Morphology and size of the product were studied by TEM. It can be seen that the cube PB nanoparticles has spontaneously formed on the surface of GO, immersion of GO in the two-component aqueous $FeCl_3 + K_3[Fe(CN)_6]$ solutions (Figure 1a). Due to abundant catechol groups of PDA film, $AuCl^{4-}$ can be adsorbed onto the surface and in situ reduced to Au NPs with addition of sodium citrate. From Figure 1b, it is clearly showed that numerous uniformly distributed Au NPs with an average size of about 10 nm were observed on the surface. This deposition method greatly improves

the repeatability and controllability for the Au NPs preparation.

Fig.1 TEM images of PB-GO (a) and Au-PDA-PB-GO (b)

The prepared GO, PB-GO and Au-PDA-PB-GO nanocomposites were analyzed using reflection FT-IR respectively, after careful washing and drying. In the spectrum of GO (curve (a) of Figure 2), the peak at 1735 cm^{-1} was assigned to the stretching vibration of C=O bond. The peaks at 3410 and 1312 cm^{-1} were assigned to the IR absorption peaks of OH. The FT-IR spectrum of PB-GO exhibits typical peaks for both GO and PB (curve b of Figure 2). The weak band at 2080 cm^{-1} showed the common characteristic of PB and its analogues, corresponding to the stretching vibration of the CN group peaks around 602 and 498 cm^{-1} could be assigned to the structure of Fe-CN-Fe. The characteristic peaks of PB indicated the formation of PB on GO. Compared with the purified PB-GO, there is a new peak of Au-PDA-PB-GO nanocomposite around 1615 cm^{-1} (curve c of Figure 2). This peak corresponds to the C=C vibration of PDA film the benzene ring moiety. The characteristic peaks indicated the formation of PDA-PB-GO nanocomposites.

Fig. 2 FT-IR spectra of GO (a), PB-GO (b) and Au-PDA-PB-GO (c)

The composition of the as-synthesized products is determined by powder X-ray diffraction (XRD) which was performed by drying the precipitate on an indium tin oxide surface in the air. Figure 3 gives the XRD patterns of GO, PB-GO and Au-PDA-PB-GO nanocomposites. The pattern for GO exhibited the diffraction peaks at $2\theta=13.45°$ and the peak correspond to the (002) plane (curve a of Figure 3). For composites in the curve b of Figure 3, new diffraction peaks at $2\theta=17.71°$, 24.93°, 35.33°, 39.86°, 50.67°, 53.88° and 56.95° and these peaks correspond to the (100), (110), (200), (210), (220), (300) and (310) planes of PB, which are the characteristic peaks of PB cubic. The characteristic peaks of PB indicated the formation of PB on GO. Compared with PB-GO, not only the XRD pattern of Au-PDA-PB-GO nanocomposite exhibits typical peaks for PB (curve c of Figure 3), there are four new peaks at $2\theta=38.18°$, 44.42°, 64.63° and 77.65° and these peaks correspond to the (111), (200), (220) and (311) planes of Au, which are the characteristic peaks of Au nanoparticles. The XRD results clearly indicated the successful formation of Au-PDA-PB-GO nanocomposite, which supporting the TEM results and IR spectrum obtained above.

Fig. 3 XRD patterns of GO (a), PB-GO (b) and Au-PDA-PB-GO (c)

3.2. Electrochemical characteristics of different modified electrodes

Figure 4 displays CVs of the different steps of modified electrodes were carried out in pH 6.5 PBS. On the bare GCE (curve a of Figure 4), no obvious redox peaks were observed. Due to the strong electrocatalytic activity of PB, an apparent pair of redox peaks on the Au-PDA-PB-GO NPs modified electrode was exhibited (curve b of Figure 4). A decrease of the peak current on anti-AFP/ Au-PDA-PB-GO NPs modified electrode in the curve c of Figure 4, which indicated anti-AFP had been successfully immobilized on the surface of the electrode. Figure 4, curve d showed that the peak current further decreased, which might be due to the fact that the macromolecular protein BSA retard the electrons transfer.

Fig.4 CVs of the different electrodes in 1/15 M PBS buffer (pH=6.5)

In the figure 4, (a) is bare GCE; (b) is Au-PDA-PB-GO/GCE; (c) is anti-AFP/Au-PDA-PB-GO/ GCE ; (d) BSA/anti-AFP/Au-PDA-PB-GO/GCE

EIS has also been used to characterize the interface conductivity of modified electrodes. The semicircle diameter in the impedance spectrum was equal to the electron-transfer resistance, R_{et}. The semicircle of Au-PDA-PB-GO NPs (curve b of Figure 5) was increased slightly than that at bare GCE (curve a of Figure 5), which might be due to the weak electrical conductivity of the PDA film. The Ret increased obviously (curve c of Figure 5), indicating the successful immobilization of the anti-AFP on the electrode. After the BSA was blocked onto the anti-AFP/ Au-PDA-PB-GO/GCE surface, the Ret further increased (curve d of Figure 5), which might because of the inhibition of electron transfer by the biomacromolecules BSA layer. The EIS results are supported by the CVs obtained above.

Fig.5 EIS of the different electrodes in 5.0 mM $Fe(CN)_6^{3-/4-}$ solution

In the figure 5, (a) is bare GCE; (b) is Au-PDA-PB-GO/GCE; (c) is anti-AFP/Au-PDA-PB-GO/ GCE; (d) is BSA/ anti-AFP/Au-PDA-PB-GO/GCE

To further confirm the control type of the reactions on the electrode, CVs of the immunosensor after incubated in 1 ng/ml AFP solution at various scan rates in 1/15 M PBS (pH 6.5) has been investigated (Figure 6). Obviously, it can be observed that the dependence of redox peak currents changed linearly with the square of root of scan rate between 20 and 300 mV/s (shown in the inset), indicating the reactions on the electrode is a diffusion controllable process.

Fig.6 CV of the proposed electrode at different scan rates (from inner to outer)

The experimental conditions in the figure 6 is 20, 30, 50, 80, 100, 120, 150, 200, 250, and 300 mV/s in 1/15 M PBS (pH 6.5) ,and the inset of figure 6 is the dependence of redox peak currents on the square root vs scan rate

3.3. Optimization of experimental conditions

The incubation temperature plays an important role in the immunoreaction on the surface of the electrode. Unsuitable incubation temperature would cause reaction uncompleted or denaturation of anti-AFP and AFP in the process. The effect of incubation temperature on the current response for the antibody–antigen immunoreaction was investigated in a range of 10–50 ℃. The current response of the immunosensor decreased with increasing temperature up to 37 ℃, while the electrochemical response increased quickly as temperature over 37 ℃. The reason may be attributed by an increase of temperature had a favorable effect on the immunoreaction and the high temperature resulted in denaturation of proteins. In this work, 20 ℃ (room temperature) was chosen under the comprehensive consideration of the response characteristic of the biomolecule and operability of the experiment.

Moreover, the immunochemical incubation time is also strongly related to the degree of reactivity. Herein, we incubated the immunosensor with 1.0 ng/ml AFP standard solution for 2, 4, 6, 8, 10, 12, 14, 16, 18, 20, 22, 25 and 30 min at room temperature, and then it was tested in 5 ml pH 6.5 PBS. The response current decreased with the incubation time up to 20 min and then leveled off slowly, which indicated an equilibration state was reached. Thus, 20 min was chosen as the optimal incubation time in the subsequent work.

The pH value of the detection solution is another important factor of the activity of the protein molecule and the stability of the electronic mediator PB. This study examined the amperometric response of the immunosensor in 5 ml in a pH range of 4.5 to 8.0 of 1/15 M PBS. It was found that the immunosensor has the largest peak current and the most sensitive response in pH 6.5. Thus, pH 6.5 of the detection solution was selected in the subsequent work.

3.4. Performance of the immunosensor

To evaluate the performance of the immunosensor, the anti-AFP/Au-PDA-PB-GO biofilm modified electrode was tested in various concentrations of AFP solutions under the optimal experimental conditions. The CVs were shown in Figure 7. The peak current obtained a further decrease with the

increment of logarithm of AFP concentration in the samples, which due to the increased hindrance of the antigen-antibody complex to electron transfer of the mediator of PB. The calibration plot for AFP detection with the proposed immunosensor under the optimal experimental conditions is illustrated in the inset of Figure 7. As a result, a linear relationship between the CV peak current and the logarithm of AFP concentration was obtained from 0.01 to 80.0 ng/ml with a regression equation : I= 7.62 * logc_{AFP}(ng/ml) +20.59 (R^2=0.9978) and a detection limit of 0.007 ng/ml at the signal-to-noise ratio of 3. The low detection limit and wide dynamic measurement range may be attributed by the Au-PDA-PB-GO NPs. The composites not only increase the loading capacity of the anti-AFP due to the large specific area of Au NPs, but also provide a favorable microenvironment to maintain the activity of the immobilized anti-AFP. Moreover, as the employment of PB and GO, the thin film immobilized on the electrode formed with Au-PDA-PB-GO NPs has excellent electrocatalytic activity.

Fig.7 CVs of different concentration of AFP

The inset of figure 7 is the peak current vs. logarithm of AFP concentration in 1/15 M PBS (pH 6.5)

3.5. Reproducibility, stability and selectivity of the immunosensor

The reproducibility of the immunosensor was evaluated. When the immunosensor was repeated under the optimal experimental conditions for five successive measurements at AFP concentration of 25.0 ng /ml, we acquired the relative standard deviation (RSD) of 3.9%. Five electrodes of different batches prepared in the same conditions present RSD of 4.1%, indicating the fine reproducibility of the immunosensor. The stability of the immunosensor was investigated. The fresh prepared immunosensor was scanned by CV for 90 continuous cycles under the optimal experimental conditions at 50 mV/s; compared with the initial value, the peak current of the 90th-cycle fallen only 4.2%. Then, it was measured every 3 days and no obvious decrease of current response during the first 10 days. In the next 20 days, it decreased only 6.8% of its initial response. The good performance may be due to the good stability and biocompatibility of the Au-PDA-PB-GO NPs.

Selectivity is the important indicators of specificity and anti-interference ability of immunosensor. In this work, we used three interfering substances: carcino-embryonic antigen (25 ng/ml), DA (25 ng/ml) and BSA (25 ng/ml) as interfering substances to evaluate the selectivity. The fresh prepared immunosensors were separately incubated 20 min with 25 ng/ml AFP solutions with interference or

without interference. The relative deviation of the current response in the two solutions is less than 4.6%, which demonstrated that the immunosensor was able to detect the AFP effectively with high specificity and anti-interference ability.

4. Conclusions

This paper reports a conspicuously simple and highly sensitive electrochemical immunosensor based on immobilization of AFP on biocompatible redox-active Au-PDA-PB-GO composites film. The multi-functional Au-PDA-PB-GO NPs were synthesized through in situ deposition of Au NPs on the PDA functionalized PB-GO nanocomposites. The Au-PDA-PB-GO nanocomposites not only enhance the stability of prussian blue and provide a favorable microenvironment to maintain the activity of the immobilized biomolecules due to the excellent biocompatibility of PDA, but also increase the loading capacity of the biomolecules due to the large surface area of nanocomposites, and the present of gold nanoparticles enhance the conductivity and charge-transport properties of the composites. The fabricated Au-PDA-PB-GO nanocomposites exhibited excellent performance as immunosensors. The low cost, simplicity in fabrication procedures, high sensitivity, good reproducibility and selectivity of the proposed immunosensor provides potential applications for clinical immunoassays.

Acknowledgement(s). This research was supported by College of Chemistry and Chemical Engineering, Shihezi University. The authors thank the Inorganic Materials Laboratory for providing the facilities and materials for this study.

References

1. H.B. El-Serag, N. Engl. J. Med., 2011, **365,** 1118.
2. Z. Altintas, I. Tothill, Sensors and Actuators B: Chemical, 2013, **188**, 988.
3. S. Mathew, A. Ali, H. Abdel-Hafiz, et al, Infect Genet Evol, 2014, **26**, 327.
4. Tothill, E. Ibtisam, Seminars in cell & developmental biology, 2009, **20**, 55.
5. W. Liang, W. Yi, S. Li, et al, Clinical biochemistry, 2009, **42**, 1524.
6. W. Jiang, R. Yuan, Y.Q. Chai, et al, Analytical biochemistry, 2010, **407**, 65.
7. X. Chen, X. Jia, J. Han, et al, Biosensors and Bioelectronics, 2013, **50**, 356.
8. H. Yang, Z. Li, X. Wei, et al, Talanta, 2013, **111**, 62.
9. L. Yan, X. Bo, D. Zhu, et al, Talanta, 2014, **120**, 304.
10. K.J. Huang, Y.J. Liu, H.B. Wang, et al, Electrochimica Acta, 2014, **118**, 130.
11. G. Lai, H. Zhang, J. Yong, et al, Biosensors and Bioelectronics, 2013, **47**, 178.
12. Z. Sun, Z. Luo, C. Gan, et al, Biosensors and Bioelectronics, 2014, **59**, 99.
13. S. Peng, G. Zou, X. Zhang, Journal of Electroanalytical Chemistry, 2012, **686**, 25.
14. Y. Wu, W. Xu, Y. Wang, et al, Electrochimica Acta, 2013, **88**, 135.
15. J. Han, J. Ma, Z. Ma, Biosensors and Bioelectronics, 2013, **47**, 243.
16. K.D. Ranjith, D. Manoj, J. Santhanalakshmi, Sensors and Actuators B: Chemical, 2013, **188**, 603.
17. F. Zhang, Y. Li, Y. Gu, et al, Microchimica Acta, 2011, **173**, 103.
18. W. Jiang, R. Yuan, Y.Q. Chai, et al, Analytical biochemistry, 2010, **407**, 65-71.
19. A. Salimi, L. Miranzadeh, R. Hallaj, Talanta, 2008, **75**, 147.
20. J. Tkáč, I. Voštiar, P. Gemeiner, E. Šturdík, Bioelectrochemistry, 2002, **55**, 149.
21. C. Hong, R. Yuan, Y. Chai, et al, Electroanalysis, 2008, **20**, 2185.
22. J.D. Qiu, H.Z. Peng, R.P. Liang, et al, Langmuir, 2007, **23**, 2133.
23. Y. Yao, X. Bai, K K.Shiu, Nanomaterials, 2012, **2**, 428.
24. C. Zhai, X. Sun, W. Zhao, et al, Biosensors and Bioelectronics, 2013, **42**, 124.
25. S. Hong, K.Y. Kim, H.J. Wook, et al, Nanomedicine, 2011, **6**, 793.
26. H. Lee, S.M. Dellatore, W.M. Miller, et al, science, 2007, **318**, 426.
27. H. Lee, J. Rho, P.B. Messersmith, Advanced Materials, 2009, **21**, 431.
28. S. Hong, Y.S. Na, S. Choi, et al, Advanced Functional Materials, 2012, **22**, 4711.
29. G. Wang, H. Huang, G. Zhang, et al, Langmuir, 2010, **27**, 1224.
30. Y. Wang, L. Liu, M. Li, et al, Biosensors and Bioelectronics, 2011, **30**, 107.
31. H. Lee, N.F. Scherer, P.B. Messersmith, Proceedings of the National Academy of Sciences, 2006, **103**, 12999.
32. B.H. Kim, D.H. Lee, J.Y. Kim, et al. Advanced Materials, 2011, **23**, 5618.
33. A.K. Geim , K.S. Novoselov, Nat. Mater, 2007, **6**,183.
34. S. Alwarappan, A. Erdem, C. Liu, et al, J. Phys. Chem. C, 2009, **113**,8853.
35. M.D. Stoller, S. Park , Y. Zhu , et al, Nano Lett., 2008, **8**, 3498.
36. X.L. Zuo，S.J. He，D. Li , et al, Langmuir, 2010, **26**, 1936.
37. L.F. Sheng, J.T. Ren, Y.Q. Miao，et a1, Biosens. Bioelectron., 2011, **26**, 3494.
38. Q. Zhang，S.Y. Wu，L. Zhang，et a1, Biosens. Bioelectron., 2011, **26**,2632 .
39. L.M. Lu，H.B. Li，F.L. Qu，et a1, Biosens. Bioelectron., 2011, **26**, 3500.
40. C.M. Willemse, K. Tlhomelang, N. Jahed, et a1, Sensors, 2011, **11**, 3970.
41. Y.Y. Shao, J. Wang, H. Wu , et al, Electroanal., 2010, **22**, 1027.
42. S. Stankovich , D.A. Dikin, GHB. Dommett, et al, Nature, 2006, **442**,282.
43. Y. Si, E.T. Samulski, Nano Lett., 2008, **8**, 1679.

44. M. Hilder, B.W. Jensen, D. Li, et al, Phys. Chem. Chem. Phys., 2011, **13**, 9187.

45. J. Han, J. Ma, Z. Ma, Biosensors and Bioelectronics, 2013, **47**, 243.

46. L. Cao, Y. Liu, B. Zhang, et al, ACS applied materials & interfaces, 2010, **2**, 2339.

47. W.S. Hummers, R.E. Offeman, Journal of the American Chemical Society, 1958, **80**, 1339.

Figure Captions

Scheme 1. Procedures for the fabrication of Au-PDA-PB-GO NPs composites(A), and the AFP immunosensor (B)

Fig. 1 TEM images of PB-GO (a) and Au-PDA-PB-GO (b)

Fig. 2 FT-IR spectra of GO (a), PB-GO (b) and Au-PDA-PB-GO (c)

Fig. 3 XRD patterns of GO (a), PB-GO (b) and Au-PDA-PB-GO (c)

Fig. 4 CVs of the different electrodes in 1/15 M PBS buffer (pH=6.5)

Fig. 5 EIS of the different electrodes in 5.0 mM $Fe(CN)_6^{3-/4-}$ solution

Fig. 6 CV of the proposed electrode at different scan rates (from inner to outer)

Fig. 7 CVs of different concentration of AFP

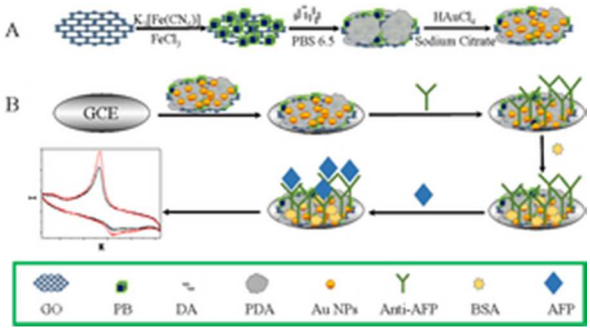

Procedures for the fabrication of Au-PDA-PB-GO NPs composites(A), and the AFP immunosensor (B)
24x13mm (300 x 300 DPI)

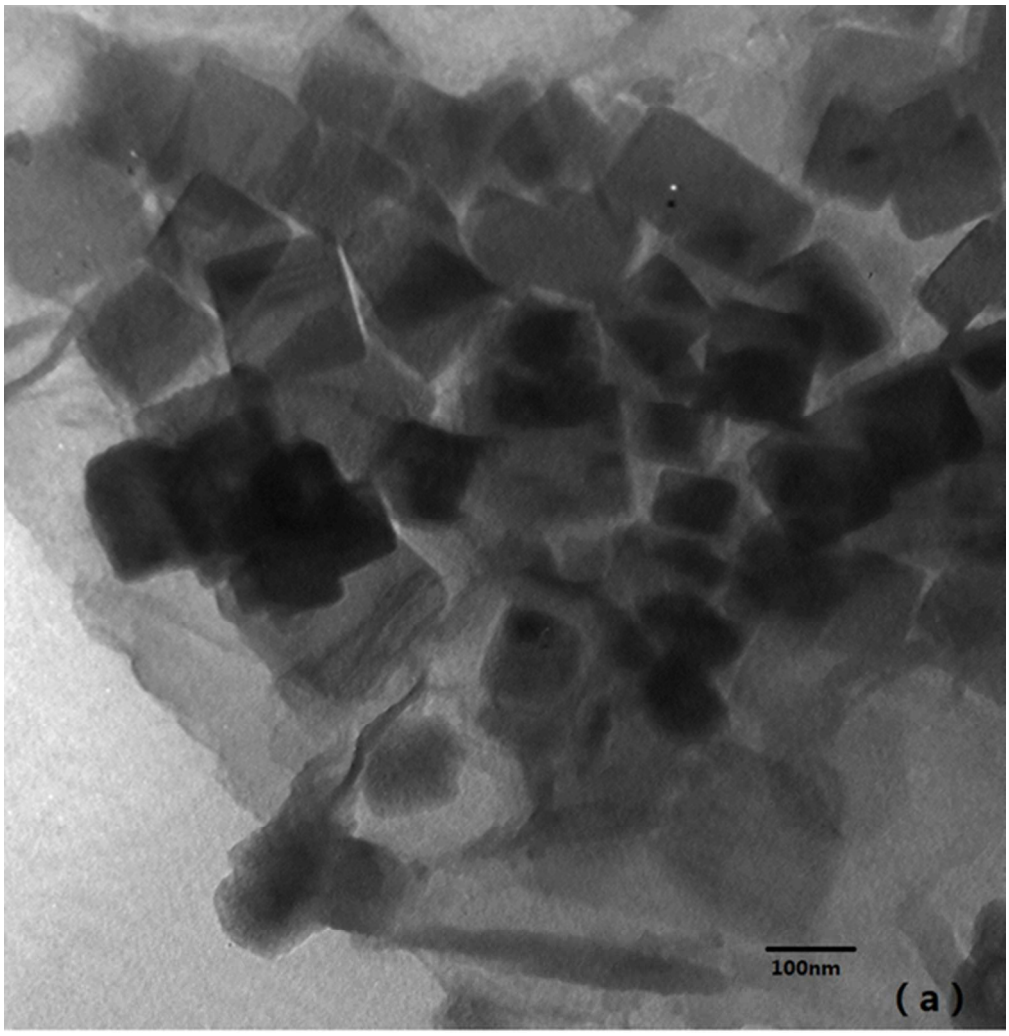

TEM images of PB-GO (a)
52x53mm (300 x 300 DPI)

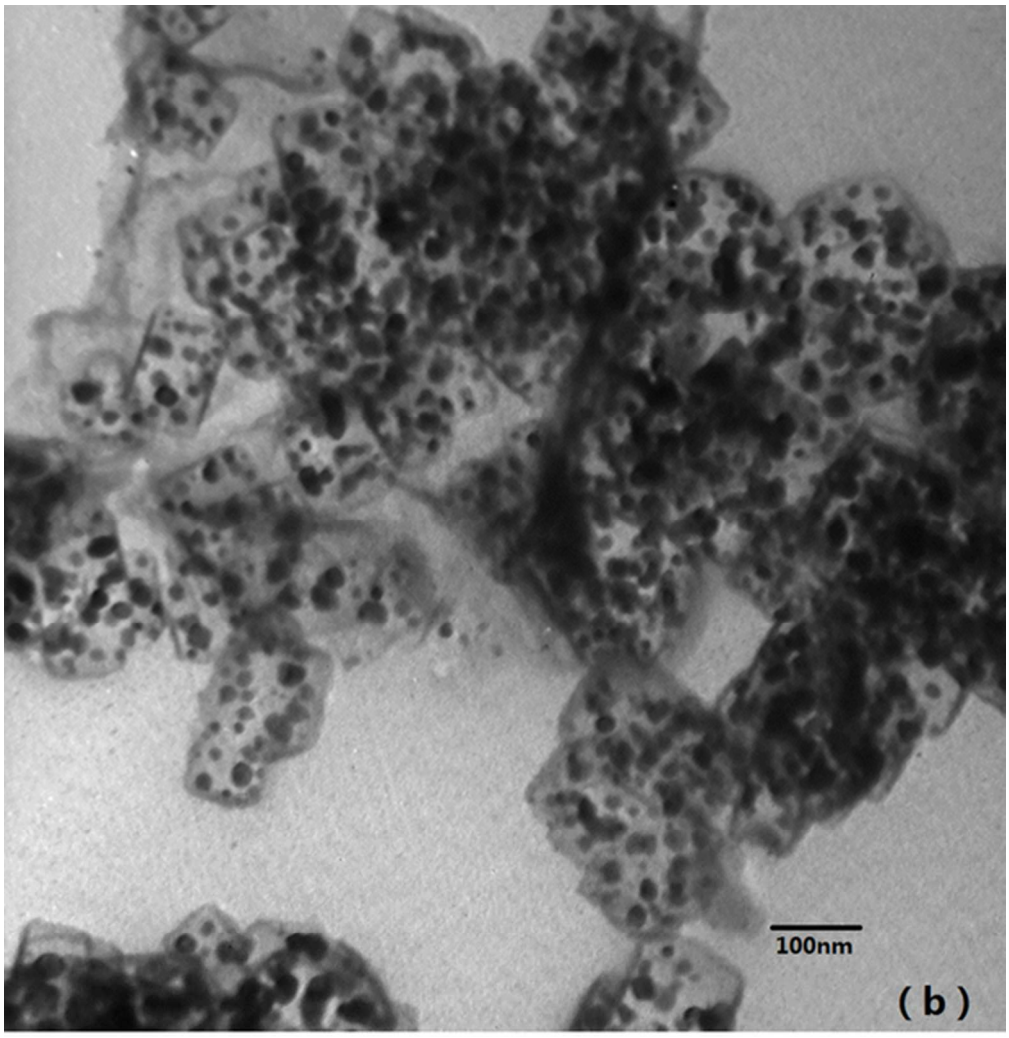

TEM images of Au-PDA-PB-GO (b)
52x53mm (300 x 300 DPI)

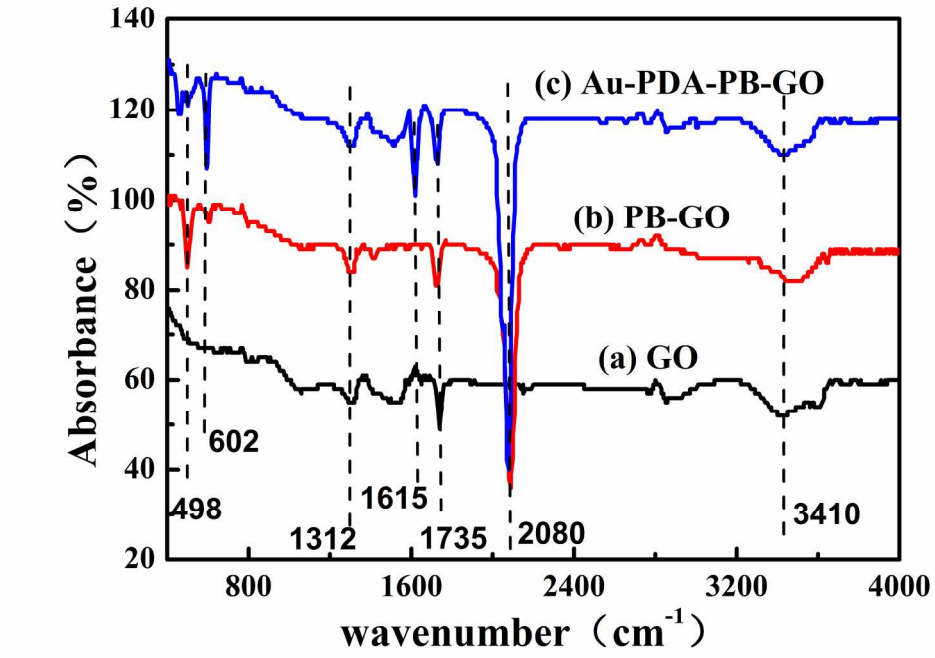

FT-IR spectra of GO (a), PB-GO (b) and Au-PDA-PB-GO (c)
214x171mm (300 x 300 DPI)

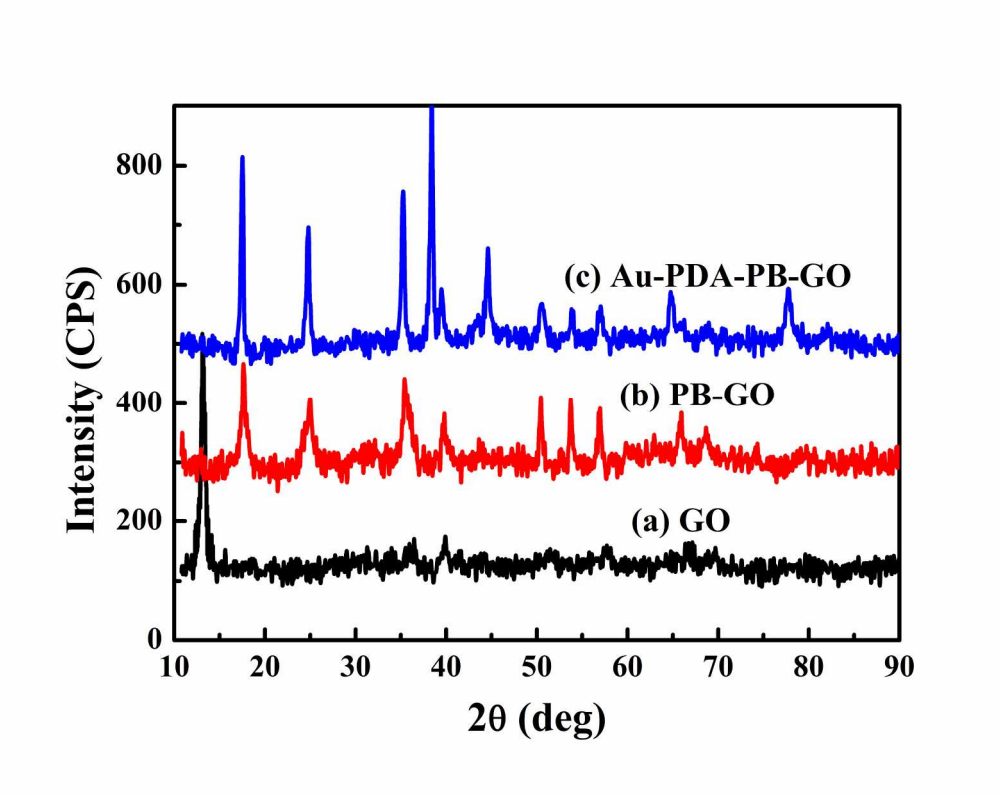

XRD patterns of GO (a), PB-GO (b) and Au-PDA-PB-GO (c)
215x171mm (300 x 300 DPI)

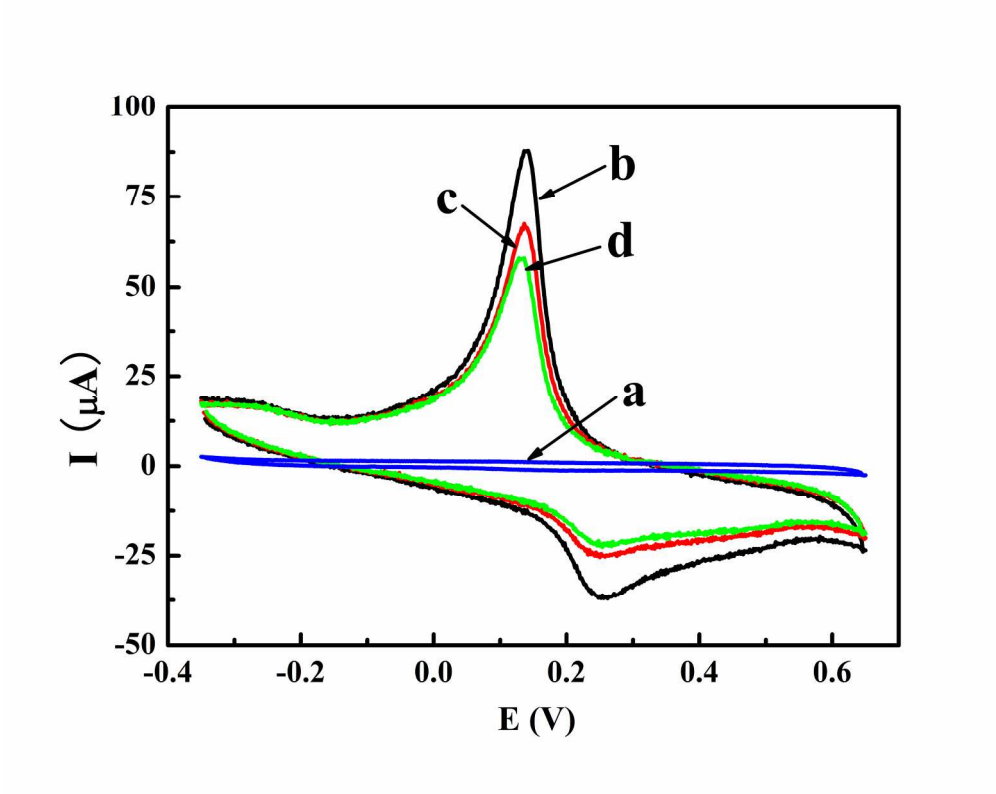

CVs of the different electrodes in 1/15 M PBS buffer (pH=6.5)
213x169mm (300 x 300 DPI)

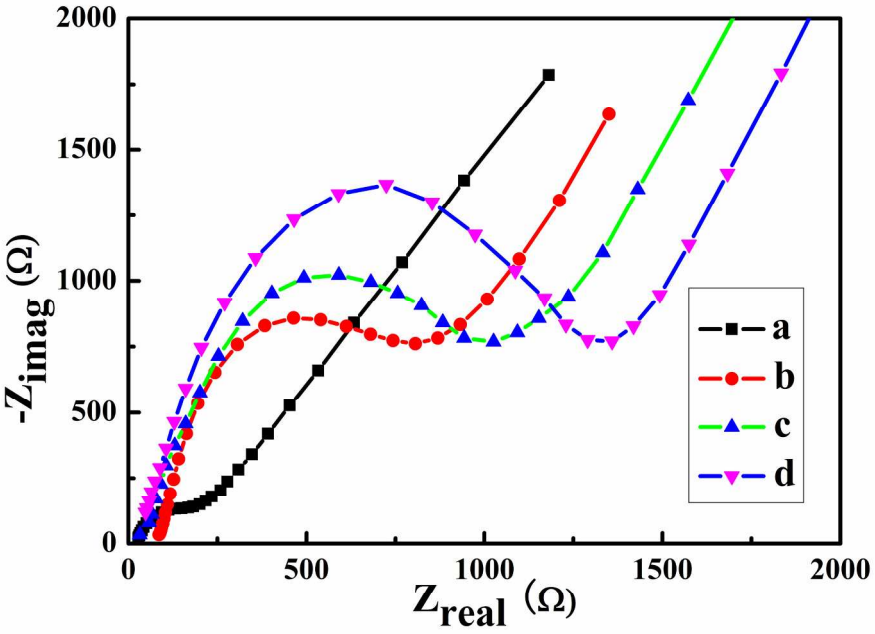

EIS of the different electrodes in 5.0 mM Fe(CN)63-/4- solution
213x165mm (300 x 300 DPI)

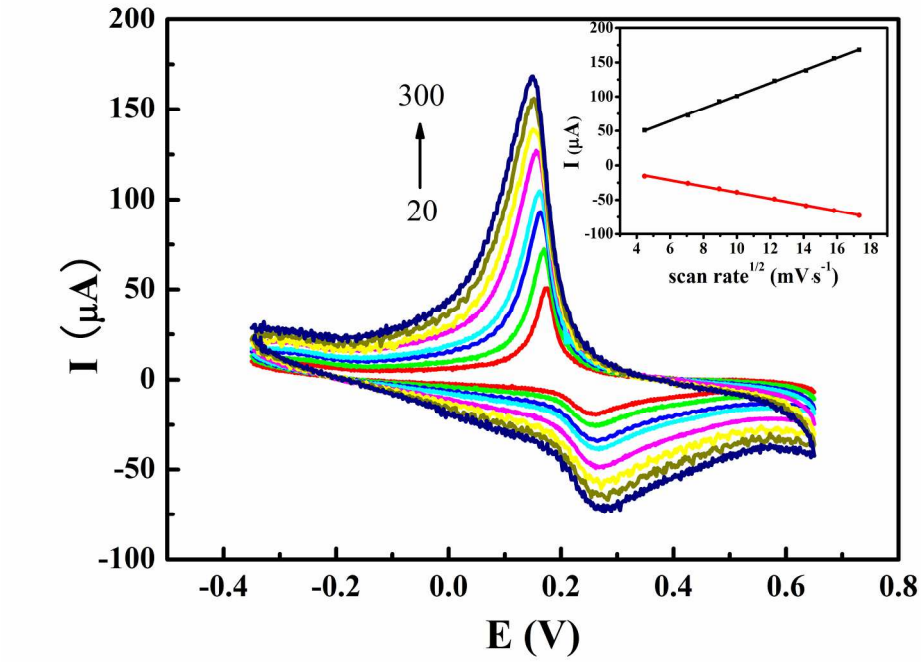

CV of the proposed electrode at different scan rates (from inner to outer)
214x172mm (300 x 300 DPI)

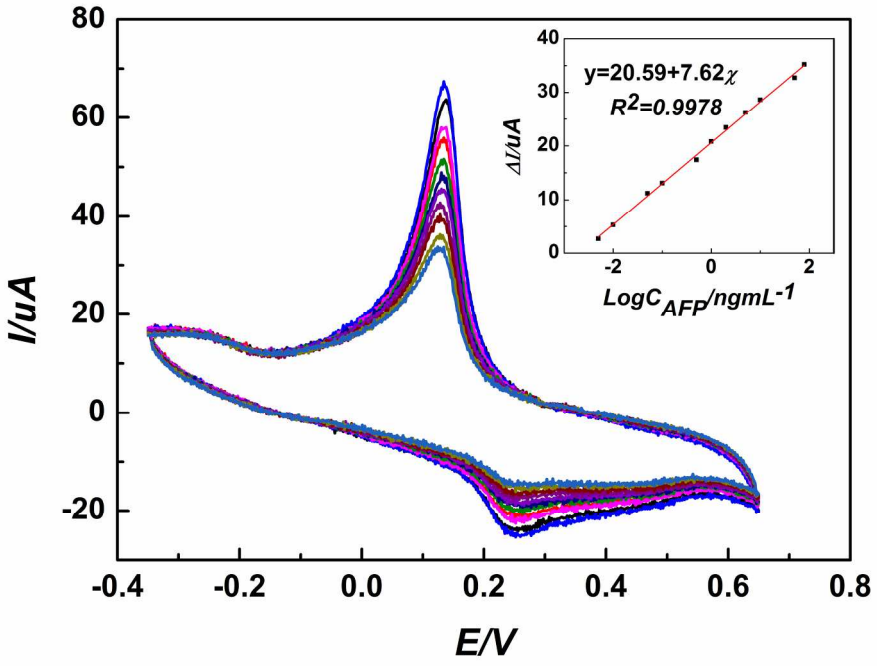

CVs of different concentration of AFP
214x172mm (300 x 300 DPI)